Power System Technology
ISSN:1000-3673

Received: 16-03-2025 *Revised: 05-04-2025* *Accepted: 22-05-2025*

Novel Flexible Arrayed Multi-Layer Eddy Current Sensor using Three-Phase Excitation for Inspecting Rail Rolling Contact Fatigue Cracks

Ahmed Chaouki Lahrech[1*], Mohamed Hichem Lahrech[1], Abdelkader Bouhlal[2], Mohamed Elbar[1]

[1] Faculty of Science and Technology, University of Djelfa, 17000 DZ, Algeria.

[2] Electrical Engineering Department. Nuclear Research Center of Birine. Djelfa, Algeria.

Correspondence Author: ahmed.lahrech@univ-djelfa.dz*

Abstract*:* -A flexible arrayed eddy current (FAEC) sensor lets you look at a big area with just one probe pass, which lets you change the shape of the part being looked at. The goal of this paper is to talk about how a flexible arrayed eddy current sensor with three-phase excitation was made to look for rolling contact fatigue (RCF) cracks in rails. Three-phase currents that are 120° out of phase power the excitation coils. The eddy current that flows through the conductive rail sample moves along in the direction of the phase variation of the excitation currents. The sensor picks up a weak background signal to verify that the rail sample doesn't have any flaws. Therefore, the sensor is highly sensitive to defects compared to other factors. Using a 3D finite element model (FEM), we look into how the sensor works. The numerical results demonstrate that the sensor can swiftly inspect and characterize steel samples from conductor rails to identify FCR defects.

Keywords*:* Eddy current nondestructive testing, Flexible arrayed sensor, three-phase excitation, Rolling contact fatigue cracks, Finite element modeling.

1. Introduction

The development of non-destructive testing (NDT) sensors aims to detect defects in materials under a variety of operating conditions with fast speed, reliable measurement, and effective cost [1]. For electrically conducting materials, structures, and subassemblies, eddy current testing (ECT) is a commonly imposed technology for maintaining specified quality standards and product norms. Non-destructive testing (NDT) for rolling contact fatigue (RCF) cracks is essential to ensure the safety of rail transport. In service, the rail often experiences high and repeated contact stresses from the wheelsets, resulting in the formation of oblique RCF cracks at the rail gauge corner and running surface. When the cracks develop into spalling, the small cracks at the bottom of the spall hole can propagate downward along the rail, leading to its lateral failure [2].

Power System Technology
ISSN:1000-3673
Received: 16-03-2025 *Revised: 05-04-2025* *Accepted: 22-05-2025*

Various non-destructive testing methods, like electromagnetic acoustic transducer (EMAT) [3], ultrasonic testing (UT) [4], and alternating current field measurement (ACFM) [5], have been used to find and describe the shapes of RCF cracks. However, it remains challenging to accurately quantify the depth of these cracks due to their clustered distribution and geometric interactions. Recently, new methods using eddy current thermography have been explored to check for defects because they allow for quick testing and clear viewing of small temperature changes, such as pulsed eddy current thermography (ECPT) [2], [6], pulsed phase eddy current thermography (ECPPT) [7], and locked eddy current thermography (ECLT) [8].

In [9], researchers developed a flexible array eddy current sensor and presented a novel excitation/detection trace design to achieve a differential and array configuration, thereby improving the reliability of non-destructive testing of the inner surfaces of hollow shafts. Recently, researchers have extensively studied hybrid probes equipped with anisotropic magnetoresistance (AMR), giant magnetoresistance (GMR), and tunnel magnetoresistance (TMR) sensors to improve the low-frequency performance and spatial resolution of ECTs [10], [11]. These sensors exhibit high magnetic sensitivity over a wide frequency range. Their disadvantages include saturation, hysteresis effects, and high cost. Rotating magnetic field ECT sensors composed of multi-excitation coils have been described in [12], [13]. Most arrayed eddy current sensors use multiplexing to excite and sense a series of individually arranged elements [14]. This approach can lead to suboptimal results. Multiplexing involves activating and deactivating coils in specific sequences to exploit the sensor's width. It also minimizes interference between neighboring coils and increases the sensor's resolution. However, its use also has drawbacks: the complexity of the multiplexing circuit increases the cost of the ECT system; switching introduces noise into the signal; and the multiplexing process affects the scanning speed.

Our contribution in this article focuses on the design of a flexible arrayed eddy current sensor using three-phase excitation to inspect rolling contact fatigue cracks in rails. The currents in the excitation coils are identical in amplitude and frequency but 120° out of phase. The eddy currents induced in the conductor rail sample are electrically offset, eliminating the need for a multiplexer. We use a sensing coil array to measure the outputs during the inspection. If the sensor is placed on a defect-free rail sample, the background signals measured by the sensing coils are small because the magnetic fields of the three-phase excitations cancel each other out. Therefore, the output is very sensitive to the eddy current disturbance caused by a defect. The physical principle and feasibility of the sensor were investigated using a finite element model (FEM) to detect defects in conductor rail samples.

Power System Technology
ISSN:1000-3673
Received: 16-03-2025 Revised: 05-04-2025 Accepted: 22-05-2025

2. Physical Principles and Sensor Design

The proposed flexible arrayed eddy current sensor is composed of several units. Each unit contains identical planar racetrack excitation coils and a pickup coil, as shown in Fig. 1(a) and (b). The currents driven in the three excitation coils are $120°$ apart in phase, e.g., assume $I_A = I_0\cos(\omega t)$, then $I_B = I_0\cos(\omega t + 120°)$, and $I_C = I_0\cos(\omega t + 240°)$, where ω is the angular frequency and I_0 is the amplitude of the currents. We position the pickup coil above the three excitation coils. The superposition principle allows us to write the output voltage of the pickup coil v_p as follows:

$$v_{\mathrm{p}} = v_{\mathrm{A}} + v_{\mathrm{B}} + v_{\mathrm{C}} \quad (1)$$

where v_{A}, v_{B}, and v_{C} represent the output voltages generated by coils A, B, and C operating independently. When the unit is placed on the sample without defect and all the conditions remain symmetric, if $v_p = v_0\cos(\omega t + \theta)$, where v_0 is the amplitude and θ is the phase angle of v_{A}, then it is derived that $v_{\mathrm{B}} = v_0\cos(\omega t + \theta + 120^{\circ})$ and $v_{\mathrm{C}} = v_0\cos(\omega t + \theta + 240^{\circ})$. So

$$v_{\mathrm{p}} = v_0[\cos(\omega t + \theta) + \cos(\omega t + \theta + 120^{\circ}) + \cos(\omega t + \theta + 240^{\circ})] = 0 \quad (2)$$

Therefore, the output voltage is zero for a defect-free sample. A defect in the sample will disrupt the eddy current distribution. Consequently, the pickup coil will measure a voltage signal. Because the background signal is zero, the defect signal abruptly appears in the output.

In other words, the sensor has a high relative sensitivity to the presence of defects. This is one of the sensor's major advantages.

Fig. 2 depicts a flexible arrayed sensor based on the three-phase excitation unit previously described. When the coils drive three-phase excitation currents, the induced voltages of the other coils differ in phase, which can partially cancel each other when summed. As a result, the background signals measured by the array sensor's pickup coils on the defect sample are smaller than those measured by the conventional array EC sensor.

3. Model-Based Performance Study

3.1 3-D FEM MODEL

A 3-D finite element model was developed to understand the physical principle and study the performance of the sensor. The formulation is based on magnetic vector potential and electric scalar potential, the gauged $A, V-A$ formulation [13]. The magnetic vector potential A is used in this formulation throughout the region $\Omega_n \cup \Omega_c$ and the electric scalar potential V only in Ω_c, where Ω_n, Ω_c, are, the eddy current free region (such as domains containing non-

Power System Technology
ISSN:1000-3673
Received: 16-03-2025 Revised: 05-04-2025 Accepted: 22-05-2025

conducting media as well as coils with known current density) and the eddy current region. The partial differential equations of an eddy current field problem, having a unique solution according to Coulomb gauge, can be written as:

$$\nabla \times (v_0 \nabla \times A) - \nabla(v_0 \nabla \cdot A) + \sigma(i\omega A + \nabla V) = 0, \ in\ \Omega_c \quad (3)$$

$$-\nabla \cdot (\sigma i\omega A + \sigma \nabla V) = 0, \ in\ \Omega_c \quad (4)$$

$$\nabla \times (v_0 v_r \nabla \times A) - \nabla(v_0 v_r \nabla \cdot A) = J_s, \ in\ \Omega_n \quad (5)$$

In (3) and (5), $v_0 = 1/\mu_0$ and $v_r = 1/\mu_r$ are, respectively, the reluctivity of vacuum and the relative reluctivity in the eddy current free region, σ is the electrical conductivity, ω is the angular frequency, and J_s is the source current density.

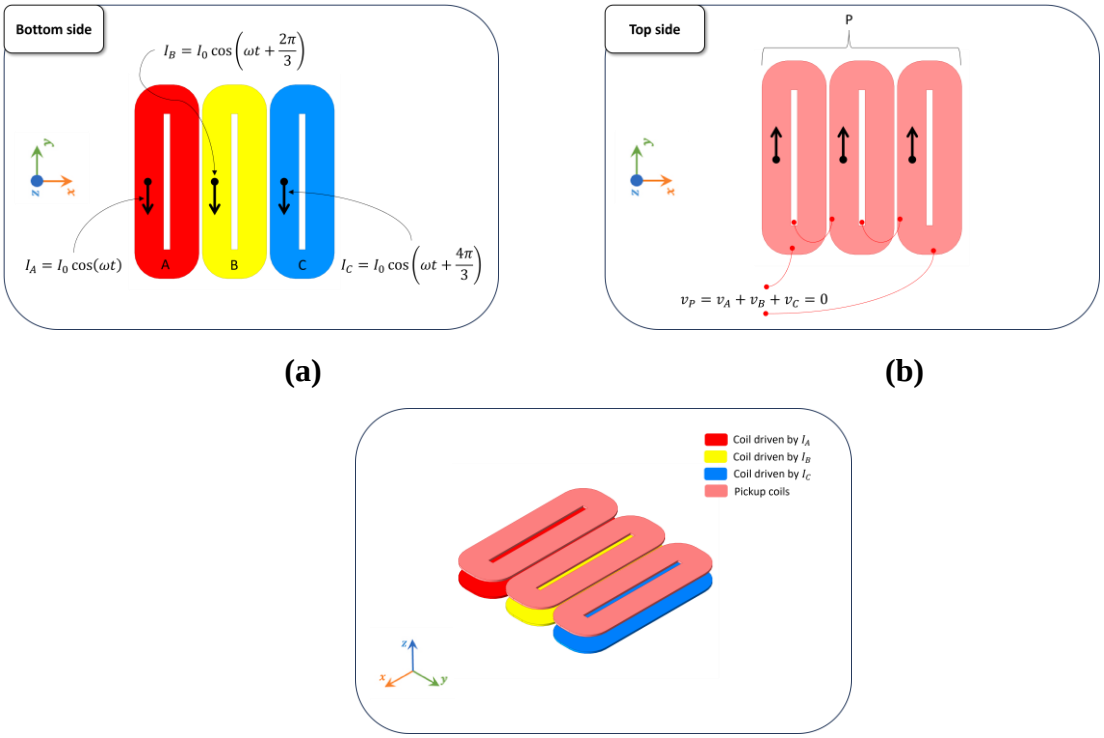

(a) **(b)**

(c)

Figure 1: (a) Bottom view of a unit of the proposed EC sensor with three-phase excitation; (b) Top view of a unit of the proposed EC sensor with pickup coil; and (c) 3D design of the proposed EC sensor with three-phase excitation and a pickup coil.

Power System Technology
ISSN:1000-3673
Received: 16-03-2025 Revised: 05-04-2025 Accepted: 22-05-2025

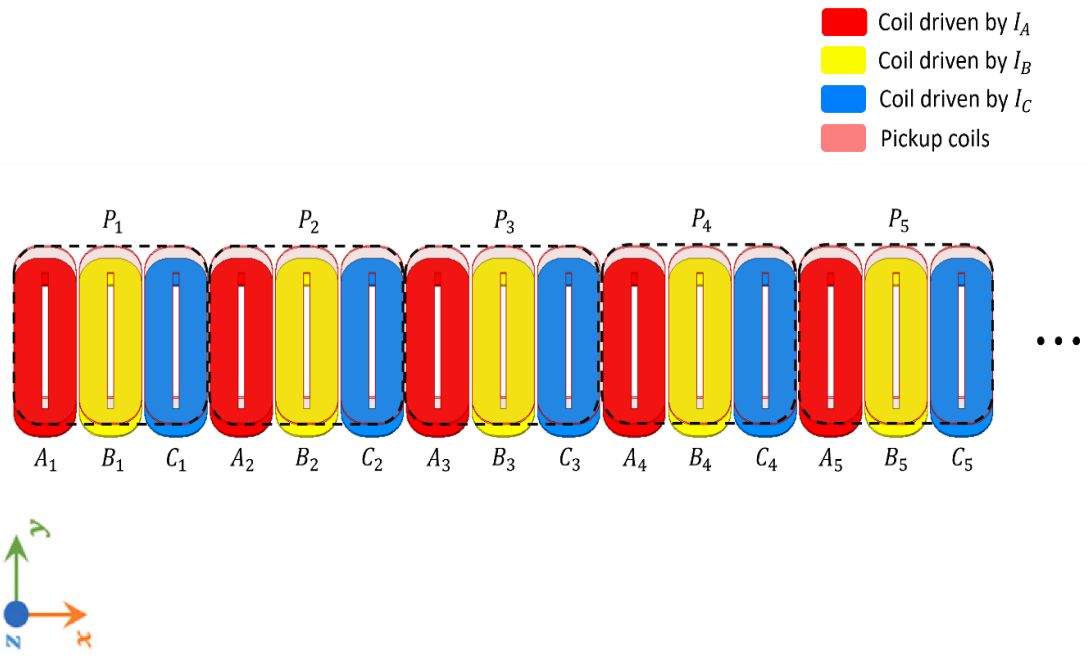

Figure 2: A flexible arrayed eddy current sensor design with three-phase excitation.

Once the magnetic vector potential A and the electric scalar potential V are determined, the induced voltage in the pickup coil is calculated using equation (6).

$$V_p = -i\omega N \iint_S B \cdot n dS = -i\omega N \oint A \cdot dl \quad (6)$$

where S is the encircling area of the pickup coil, n is the outward normal direction of the coil plane, and N is the number of the coil turns.

3.2 Model Setup and Parameters

We set the model parameters to match those in the numerical model. The number of turns for each coil is 20. The wire spacing is 0.1 mm. The length of the coil straight part and the outer width of the coil straight part of the racetrack coils are 4.2 mm and 2 mm, respectively. The distance between the centers of two adjacent excitation coils is 2.1 mm. The current amplitude driven by the three excitation coils is $I_0 = 250\ mA$, and the frequency of the excitation current is 20 kHz.

Power System Technology
ISSN:1000-3673
Received: 16-03-2025 Revised: 05-04-2025 Accepted: 22-05-2025

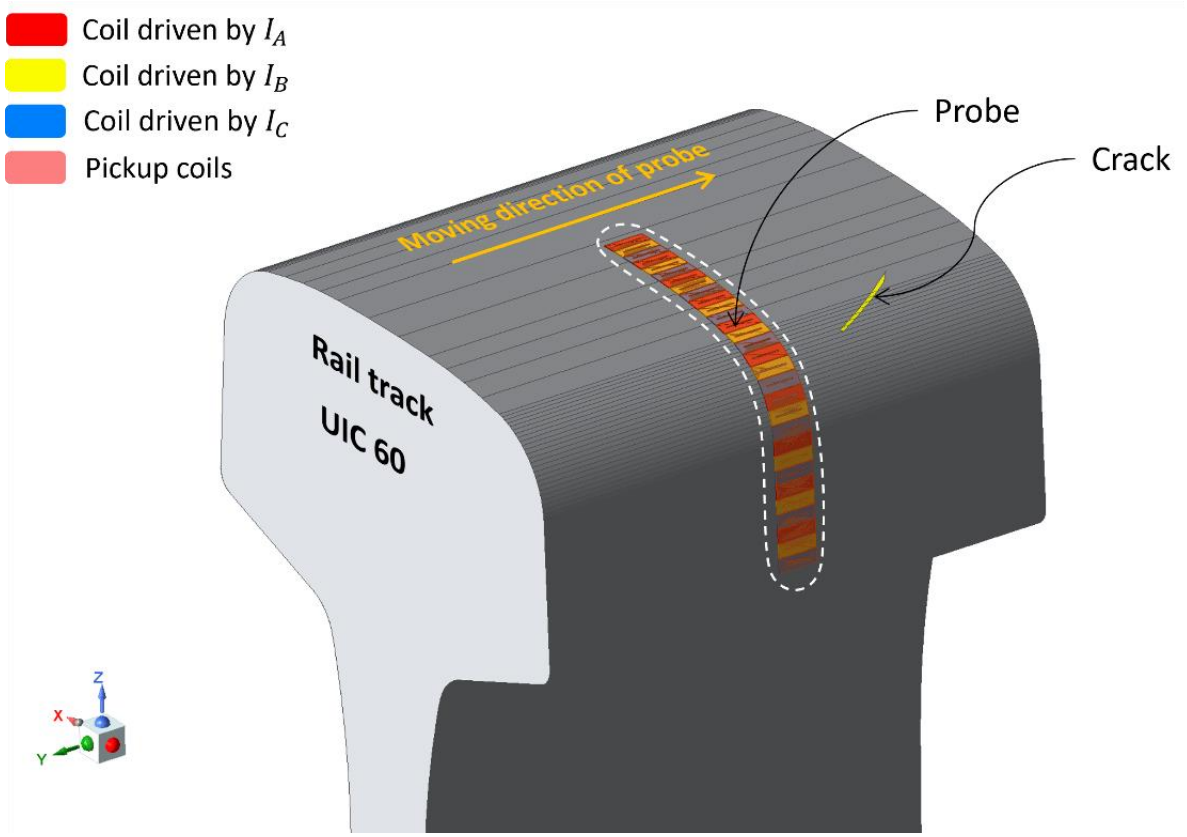

Figure 3: Schematic diagram of simulation model.

We modeled the UIC60-type rail sample with surface cracks on the rail head due to the rolling contact fatigue (RCF) of the rail steel. The rail steel sample's conductivity, relative permeability, and relative permittivity are 1.2×10^6 (S/m), 400, and 1, respectively. As shown in Fig. 3, we use a Cartesian coordinate system with an origin at the top surface of the rail head sample and a z-axis perpendicular to the surface. The flexible arrayed eddy current sensor's lift-off to the rail steel sample's top surface is 0.15 mm. In the simulations, the flexible arrayed eddy current sensor scans along the y-axis direction from −20 mm to 15 mm. Fig. 4(a) displays the dimensions of the UIC60-type rail sample.

Power System Technology
ISSN:1000-3673
Received: 16-03-2025 Revised: 05-04-2025 Accepted: 22-05-2025

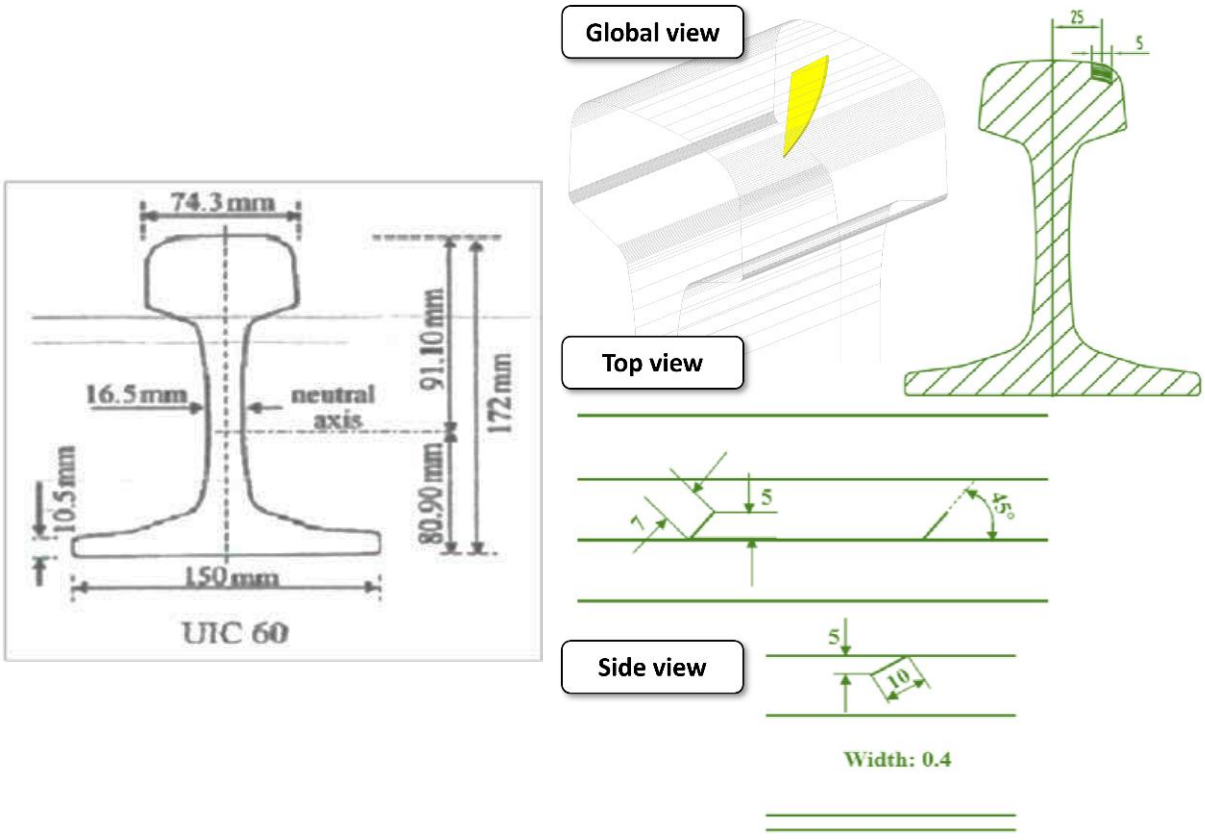

(a) **(b)**

Figure 4: (a) UIC60 rail dimensions; (b) Schematic diagram of crack dimension (5 mm depth).

This paper uses artificial cracks on the rail surface, rolled by the train, to simulate idealized rolling contact fatigue (RCF) cracks. The group of cracks is 45° to the train running direction, 30° to the horizontal plane, and the length of the crack on the tread is 5 mm, as shown in Fig. 4(b). The crack depths range from 1.00 mm to 8.00 mm. Table 1 displays the detailed dimensions of the cracks.

Table 1: Crack dimension at different depth.

Crack number	#1	#2	#3	#4	#5
lengths on the tread (mm)	5	16	7	10	25
Width (mm)	0.4	0.2	0.4	0.4	0.4
Crack depth (mm)	5.00	3.00	8.00	2.00	1.00

Power System Technology
ISSN:1000-3673
Received: 16-03-2025 Revised: 05-04-2025 Accepted: 22-05-2025

3.3 Induced Eddy Current

Fig. 5 displays the waveform of the three-phase excitation currents. The excitation currents I_A, I_B, and I_C alternately reach their maximum value. As a result, the induced eddy currents under the three-phase coils alternately reach their peak. Meanwhile, the three-phase coil positions alternate. Therefore, we deduce that the induced eddy current causes an electrical shift in the conductive rail sample.

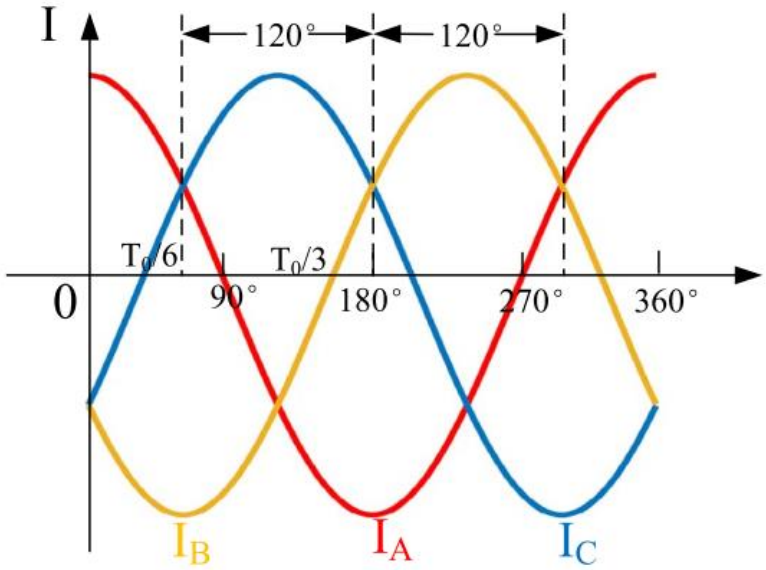

Figure 5: Waveform of the three-phase excitation currents.

We studied the induced eddy current in the conductive rail sample using the FEM model to verify this inference. Fig. 6 (a)~(e) shows the induced eddy current at five consecutive times: 0, $T_0/12$, $T_0/6$, $T_0/4$, and $T_0/3$, where $T_0 = 1/f$ is the period of the excitation current. Here, we present the induced eddy current in z.

Using excitation coils A_1, B_1, and C_1, we observe that the induced eddy current moves from A_1 to B_1 and subsequently to C_1. The circuit system of this flexible arrayed eddy current sensor is much simpler than that of other array probes because the induced eddy current moves electrically in space. It also implies that this probe can scan at a faster speed.

Power System Technology
ISSN:1000-3673
Received: 16-03-2025 *Revised: 05-04-2025* *Accepted: 22-05-2025*

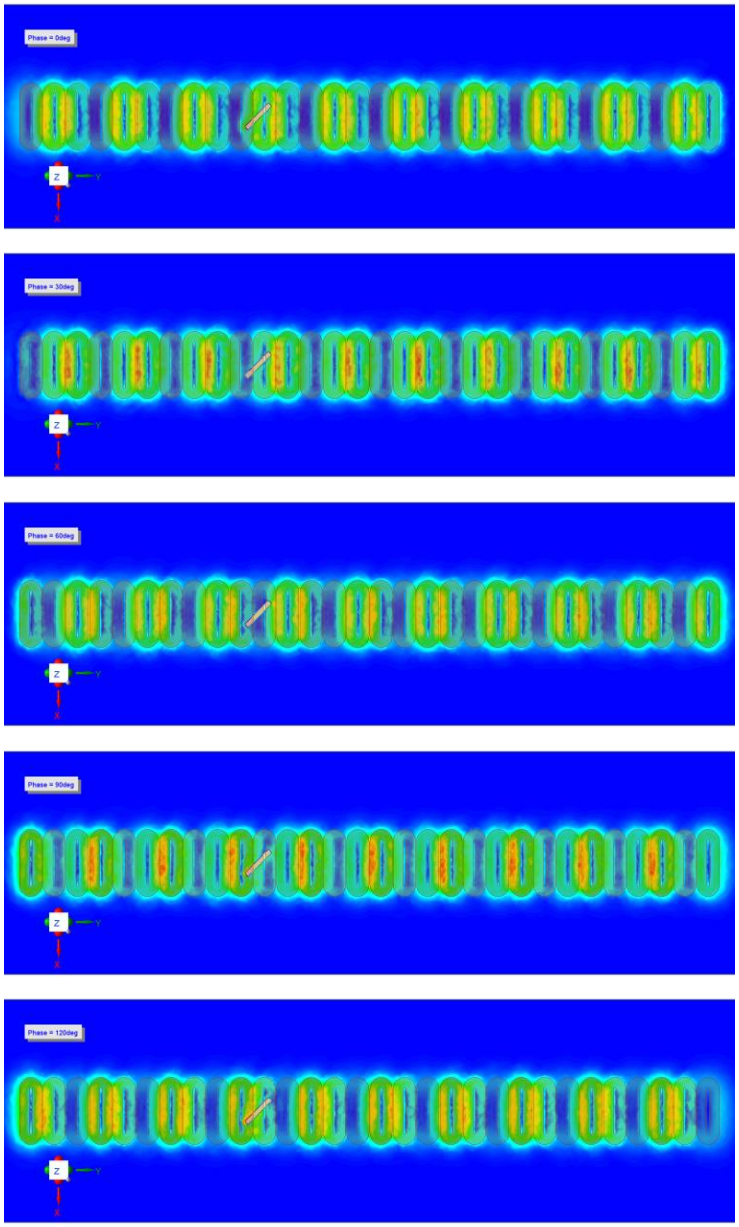

Figure 6: Simulation result: induced eddy currents in the conductive rail sample at five consecutive time: (a) 0; (b) $T_0/12$; (c) $T_0/6$; (d) $T_0/4$; (e) $T_0/3$.

4. Simulation Results

We studied the output voltages of the pickup coils using the FEM model. We modeled the output of a flexible arrayed sensor unit before delving into the flexible arrayed eddy current sensor. Three conditions were studied: (i) rail sample with #1 defect; (ii) rail sample with #5 defect; and (iii) defect-free rail sample. As shown in Table 1, defects #1 and #5 have different

Power System Technology
ISSN:1000-3673
Received: 16-03-2025 Revised: 05-04-2025 Accepted: 22-05-2025

lengths on the tread, as well as different depths. We moved the unit in Fig. 3 along the y-axis from approximately 20 mm to 15 mm, with a lift-off of 0.15 mm.

Fig. 7 presents the amplitudes of the output voltages. It is seen that the curve of the defect-free sample, that is, curve (iii) in Fig. 7, is almost zero, which confirms that the background signal measured in the defect-free area is null. Moreover, the curves (i) and (ii) show that the sensor is sensitive to both defects. The amplitude and size of the output depend on the defect lengths on the tread as well as different depths, which is helpful for defect characterization.

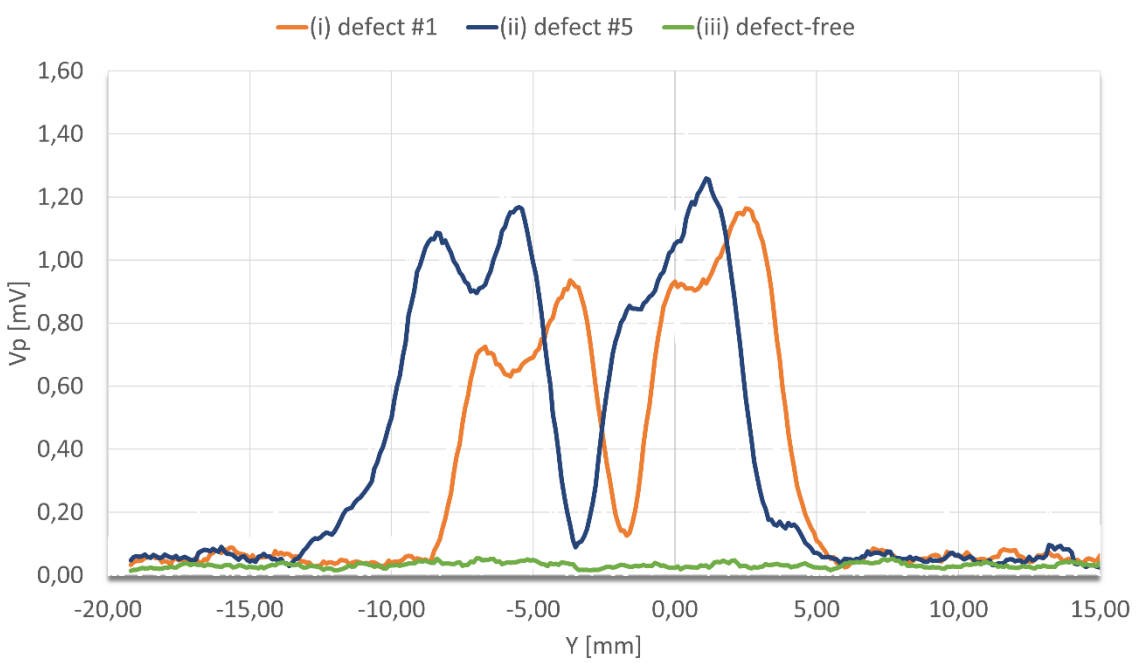

Figure 7: Simulation result: the output of the unit for 3 different conditions: i) rail sample with #1 defect; ii) rail sample with #5 defect; and iii) defect-free.

As shown in Table 1, defects #2 to #4 have different lengths and depths. Fig. 8 shows the amplitudes of the output voltages of the flexible arrayed eddy current sensor's 5th pickup coil. We observe that as the defect length increases between 7 mm, 10 mm, and 16 mm, the amplitude and size of the defect signal also increase.

Power System Technology
ISSN:1000-3673
Received: 16-03-2025 Revised: 05-04-2025 Accepted: 22-05-2025

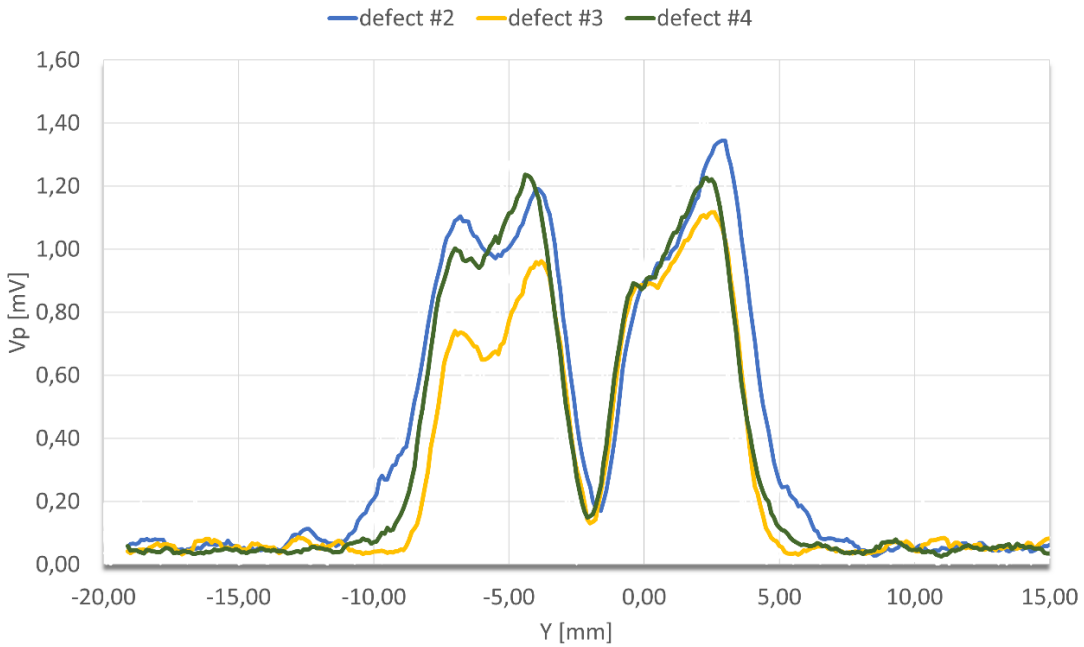

Figure 8: Simulation result: the output of the 5th pickup coil in the flexible arrayed sensor for 3 different defects: defect #2, defect #3, and defect #4.

We simulated the output of the flexible arrayed eddy current sensor. The flexible arrayed sensor has 30 excitation coils and 10 pickup coils. Fig. 9 shows the output voltages of defect #5's flexible arrayed eddy current sensor. We observe that the output voltages of the 3th, 4th, 5th, and 6th pickup coils of the flexible arrayed eddy current sensor are sensitive to defect #5.

Fig. 10 shows the output voltages of defect #2's flexible arrayed eddy current sensor. We observe that the output voltages of the 4th, 5th, and 6th pickup coils of the flexible arrayed eddy current sensor are sensitive to defect #2.

As a result, we conclude that flexible arrayed eddy current sensors have a much higher defect sensitivity compared to conventional eddy current testing sensors.

Power System Technology
ISSN:1000-3673
Received: 16-03-2025 Revised: 05-04-2025 Accepted: 22-05-2025

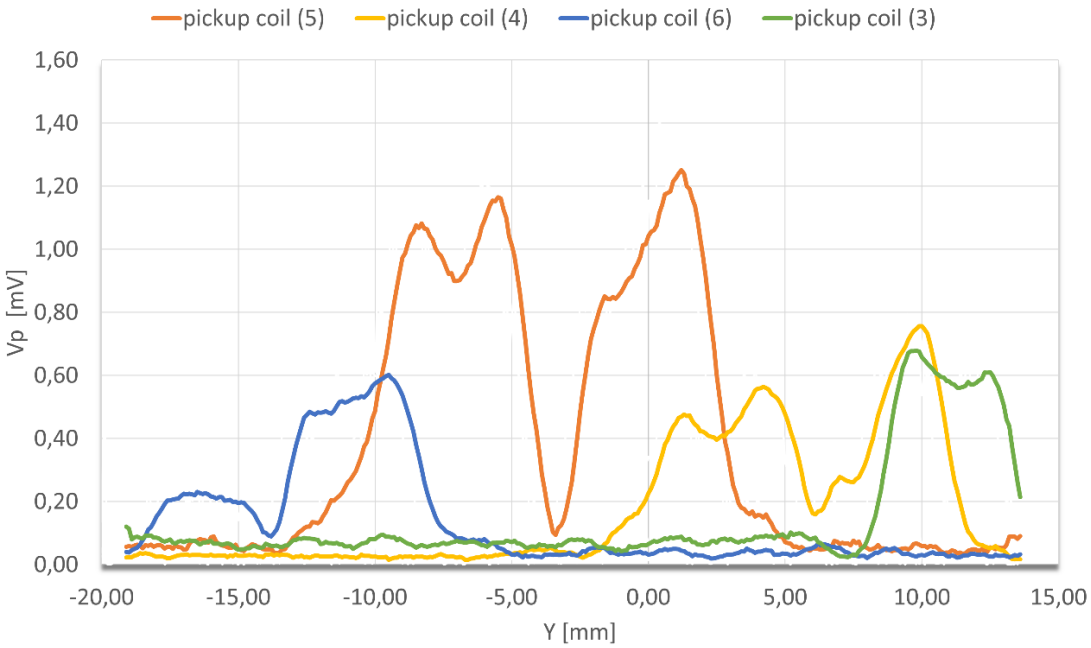

Figure 9: Simulation result: the output voltages of the 3th, 4th, 5th, and 6th pickup coils in the flexible arrayed EC sensor for defect #5.

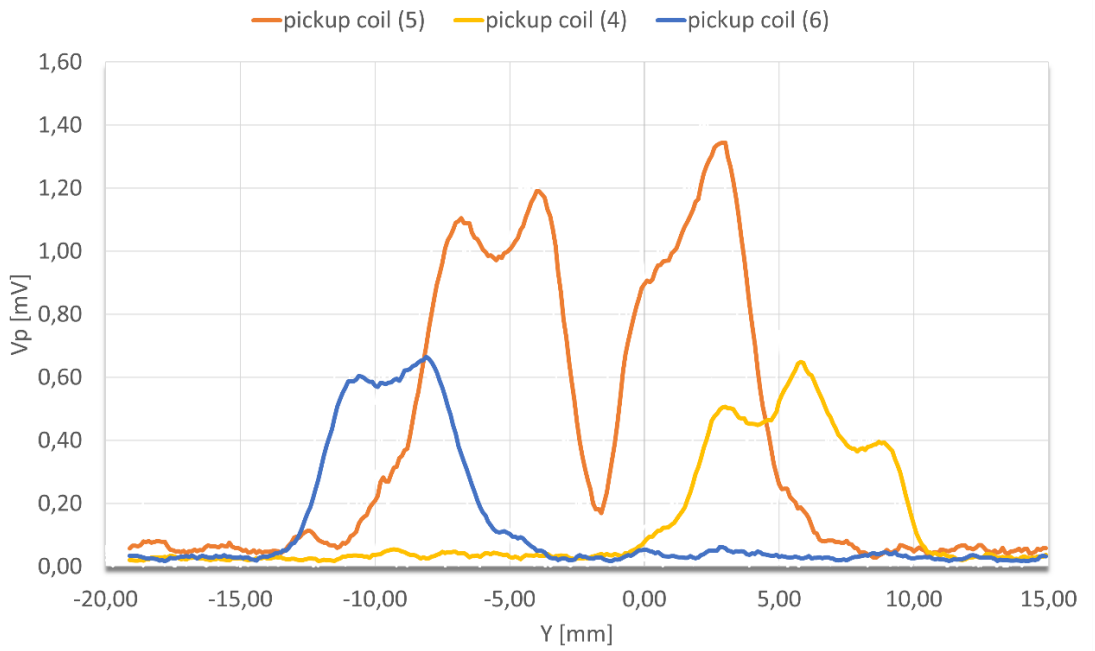

Figure 10: Simulation result: the output voltages of the 3th, 4th, 5th, and 6th pickup coils in the flexible arrayed EC sensor for defect #2.

Power System Technology
ISSN:1000-3673
Received: 16-03-2025 Revised: 05-04-2025 Accepted: 22-05-2025

5. Conclusion

A new concept of a flexible arrayed eddy current sensor that uses three-phase excitation is proposed, having the ability to inspect rolling contact fatigue cracks in rail. The operation principle and defect signals of the flexible arrayed eddy current sensor were simulated using a 3D FEM model. It is found that the induced eddy current shifts electrically in the conductive rail sample. Therefore, the flexible arrayed eddy current sensor does not require a multiplexer. As a result, this flexible arrayed sensor's excitation system is much simpler than a conventional array sensor with a multiplexer, and the scan speed can be faster. The background signal of the sensor measured on top of the defect-free rail sample is about 10 μV, which is much smaller than the signal of the defect with dimensions of (length × width × depth = 5 mm × 0.15 mm × 0.35 mm). The sensor has a significantly higher defect sensitivity than conventional eddy current testing sensors.

References

[1] N. Zhang, C. Ye, L. Peng, and Y. Tao, "Novel Array Eddy Current Sensor With Three-Phase Excitation," *IEEE Sensors Journal*, vol. 19, no. 18, pp. 7896–7905, Sep. 2019, doi: 10.1109/JSEN.2019.2919661.

[2] Y. Liu *et al.*, "Depth quantification of rolling contact fatigue crack using skewness of eddy current pulsed thermography in stationary and scanning modes," *NDT & E International*, vol. 128, p. 102630, Jun. 2022, doi: 10.1016/j.ndteint.2022.102630.

[3] C. B. Thring, Y. Fan, and R. S. Edwards, "Multi-coil focused EMAT for characterisation of surface-breaking defects of arbitrary orientation," *NDT & E International*, vol. 88, pp. 1–7, Jun. 2017, doi: 10.1016/j.ndteint.2017.02.005.

[4] L. Zhou, H. P. Brunskill, and R. Lewis, "Real-time non-invasive measurement and monitoring of wheel–rail contact using ultrasonic reflectometry," *Structural Health Monitoring*, vol. 18, no. 5–6, pp. 1953–1965, Nov. 2019, doi: 10.1177/1475921719829882.

[5] H. Rowshandel, G. L. Nicholson, J. L. Shen, and C. L. Davis, "Characterisation of clustered cracks using an ACFM sensor and application of an artificial neural network," *NDT & E International*, vol. 98, pp. 80–88, Sep. 2018, doi: 10.1016/j.ndteint.2018.04.007.

[6] J. Zhu *et al.*, "Characterization of Rolling Contact Fatigue Cracks in Rails by Eddy Current Pulsed Thermography," *IEEE Transactions on Industrial Informatics*, vol. 17, no. 4, pp. 2307–2315, Apr. 2021, doi: 10.1109/TII.2020.3003335.

Power System Technology
ISSN:1000-3673
Received: 16-03-2025 Revised: 05-04-2025 Accepted: 22-05-2025

[7] M. Ishikawa, H. Hatta, Y. Habuka, R. Fukui, and S. Utsunomiya, "Detecting deeper defects using pulse phase thermography," *Infrared Physics & Technology*, vol. 57, pp. 42–49, Mar. 2013, doi: 10.1016/j.infrared.2012.11.009.

[8] T. Sakagami and S. Kubo, "Applications of pulse heating thermography and lock-in thermography to quantitative nondestructive evaluations," *Infrared Physics & Technology*, vol. 43, no. 3, pp. 211–218, Jun. 2002, doi: 10.1016/S1350-4495(02)00141-X.

[9] Z. Sun, D. Cai, C. Zou, W. Zhang, and Q. Chen, "Design and optimization of a flexible arrayed eddy current sensor," *Meas. Sci. Technol.*, vol. 28, no. 4, p. 045105, Feb. 2017, doi: 10.1088/1361-6501/aa5b76.

[10] T. Chen, Y. He, and J. Du, "A High-Sensitivity Flexible Eddy Current Array Sensor for Crack Monitoring of Welded Structures under Varying Environment," *Sensors*, vol. 18, no. 6, Art. no. 6, Jun. 2018, doi: 10.3390/s18061780.

[11] C. Ye, Y. Wang, and Y. Tao, "High-Density Large-Scale TMR Sensor Array for Magnetic Field Imaging," *IEEE Transactions on Instrumentation and Measurement*, vol. 68, no. 7, pp. 2594–2601, Jul. 2019, doi: 10.1109/TIM.2018.2866299.

[12] A. C. Lahrech, B. Abdelhadi, M. Feliachi, A. Zaoui, and M. Naïdjate, "Electrical conductivity identification of a carbon fiber composite material plate using a rotating magnetic field and multi-coil eddy current sensor," *Eur. Phys. J. Appl. Phys.*, vol. 83, no. 2, Art. no. 2, Aug. 2018, doi: 10.1051/epjap/2018170411.

[13] A. C. Lahrech *et al.*, "Development of an axial rotating magnetic field multi-coil eddy current sensor for electromagnetic characterization of stratified CFRP materials," *NDT & E International*, vol. 126, p. 102589, Mar. 2022, doi: 10.1016/j.ndteint.2021.102589.

[14] A. McNab and J. Thomson, "An eddy current array instrument for application on ferritic welds," *NDT & E International*, vol. 28, no. 2, pp. 103–112, Apr. 1995, doi: 10.1016/0963-8695(94)00009-9.